JOURNAL OF MORPHOLOGY 270:954–965 (2009)

Turning Maneuvers in Sharks: Predicting Body Curvature From Axial Morphology

Marianne E. Porter,[1]* Cassandra M. Roque,[2] and John H. Long Jr.[1]

[1]*Biology Department, Vassar College, Poughkeepsie, New York 12604*
[2]*Comparative and Evolutionary Physiology, Department of Ecology and Evolutionary Biology, University of California, Irvine, California, 92697-2525*

ABSTRACT Given the diversity of vertebral morphologies among fishes, it is tempting to propose causal links between axial morphology and body curvature. We propose that shape and size of the vertebrae, intervertebral joints, and the body will more accurately predict differences in body curvature during swimming rather than a single meristic such as total vertebral number alone. We examined the correlation between morphological features and maximum body curvature seen during routine turns in five species of shark: *Triakis semifasciata*, *Heterodontus francisci*, *Chiloscyllium plagiosum*, *Chiloscyllium punctatum*, and *Hemiscyllium ocellatum*. We quantified overall body curvature using three different metrics. From a separate group of size-matched individuals, we measured 16 morphological features from precaudal vertebrae and the body. As predicted, a larger pool of morphological features yielded a more robust prediction of maximal body curvature than vertebral number alone. Stepwise linear regression showed that up to 11 features were significant predictors of the three measures of body curvature, yielding highly significant multiple regressions with r^2 values of 0.523, 0.537, and 0.584. The second moment of area of the centrum was always the best predictor, followed by either centrum length or transverse height. Ranking as the fifth most important variable in three different models, the body's total length, fineness ratio, and width were the most important nonvertebral morphologies. Without considering the effects of muscle activity, these correlations suggest a dominant role for the vertebral column in providing the passive mechanical properties of the body that control, in part, body curvature during swimming. J. Morphol. 270:954–965, 2009.

KEY WORDS: turning; shark; body curvature; morphology; vertebral column

INTRODUCTION

During swimming in fish-like craniates, body curvature appears to be influenced by the nonmuscular mechanical properties of the axial skeleton, present as either a notochord or a vertebral column (Long, 1995; Brainerd and Patek, 1998; Long et al., 2002). In some cases, the body's curvature is mediated by the axial skeleton's mechanical properties and is correlated with the number of vertebrae (Lindsey, 1978; Long and Nipper, 1996; Brainerd and Patek, 1998). However, the simple relation between the number of vertebrae, axial flexibility, and body curvature has been called into question in sharks, where three species of Carcharhiniformes were found to have body curvature during turning that correlated not with number of vertebrae but rather with body shape (Kajiura et al., 2003).

If this lack of correlation between the number of vertebrae and body curvature holds for sharks in general, one hypothesis is that sharks have a substantially different axial musculo-skeletal system compared with bony fishes, with the body-shape effect (Kajiura et al., 2003) mediated by the activity of the muscles (Donley et al., 2004; Bernal et al., 2005). An alternative hypothesis is that the number of vertebrae is only one of many nonmuscular features that controls body curvature. To test these alternatives, we examined the correlations between numerous morphological features of the axial skeleton and the body with the curvature of the body during routine turning in five species of sharks from three different families.

We selected candidate morphological features using information from previous work on axial morphology and beam theory from engineering. For example, in many groups of elongated actinopterygian fishes, number and fineness ratio (length: width) of the vertebral centra were predictors of body morphology (Ward and Brainerd, 2007). In sharks, centrum length differs dramatically within and among individuals (Springer and Garrick, 1964). Furthermore, the intervertebral joints are another feature of vertebral column morphology that differs within and among species and appears to be related to body flexibility (Long,

*Correspondence to: Marianne E. Porter, Biology Department, Vassar College, 124 Raymond Ave., Box 731, Poughkeepsie, NY 12604, USA. E-mail: meporter@vassar.edu

Received 7 July 2008; Revised 9 December 2008; Accepted 3 January 2009

Published online 26 February 2009 in Wiley InterScience (www.interscience.wiley.com)
DOI: 10.1002/jmor.10732

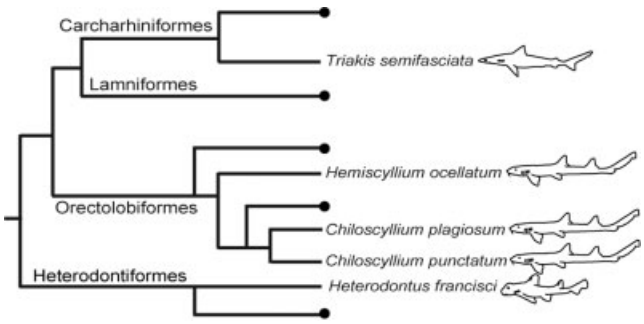

Fig. 1. Phylogenetic distribution of study species, five galeomorphs from three orders [Adapted From Maisey et al., (2004) Mesozoic Fishes 3-Systematics, Paleoenvironments, and Biodiversity, 2004, Vol. 3, pp 17–56, Verlag]. For sample sizes, see Table 1.

1992; Domenici et al., 2004). In addition, engineering beam theory suggests that for both the vertebral column and the body a key feature to measure is the second moment of area I, (in units of m^4), which is the nonlinear contribution of cross-sectional area to the flexural stiffness of the beam (Wainwright et al., 1976; Summers and Long, 2006). Finally, the body itself can also be characterized by standard measures such as length and width. The ratio of those two measures yields a fineness ratio of the body, which is related to the body's added mass coefficient during unsteady swimming (Daniel, 1984).

Quantifying maximum body curvature during turning maneuvers is problematic for at least three reasons: (1) no single metric is the obvious choice to summarize the complex spatial and temporal kinematics of axial undulation (Root et al., 2007), (2) curvature maxima vary in time and position along the body axis, and (3) curvature maxima are difficult to measure since one is rarely certain that maximal effort has been exerted by the animal (Herrel et al., 2001). Given these limitations, we chose to quantify average maximal curvature during turning maneuvers as a bending coefficient, BC, the ratio of the distance between the rostrum and a point on the caudal fin tip (BC_1) or peduncle (BC_2) to the overall length of the shark (please note that Appendix A contains a list of abbreviations used in this study) (Brainerd and Patek, 1998; Azizi and Landberg, 2002; Kajiura et al., 2003). We also used minimum bending angle (MBA) as the angle formed from the tip of the rostrum to the base of the first dorsal fin to the tip of the caudal fin (Kajiura and Holland, 2002).

We examined body curvature during turning as a function of morphology as measured in five galeomorph shark species (Fig. 1 and Table 1). We used kinematic data from swimming sharks and morphological data sets obtained from radiographs of live and preserved specimens (see Fig. 1). Our goals were as follows: (1) determine the body curvature of sharks during turning; (2) examine morphological differences in the vertebral column and the body among species; and (3) determine whether body curvature is predicted by body shape, body size, and/or vertebral morphology. We hypothesized that aspects of the vertebral centra morphology and shape of the shark's body would be significant predictors of body curvature during turning.

MATERIALS AND METHODS

Study Animals

We examined galeomorph sharks representing three families (Fig. 1, Table 1, Appendix B). We used one species from the Order Heterodontiformes, the horn shark (*Heterodontus francisci:* Heterodontidae), which is a nocturnal, benthic species. We examined one species in the Order Carcharhiniformes (Compagno, 1984, 2003), the leopard shark (*Triakis semifasciata*: Triakidae), which is an active swimmer who can also be found resting on the bottom (Webb, 1975; Donley and Shadwick, 2003). From the Order Orectolobiformes, we examined three species, all from the Hemiscylliidae, a family of largely inactive swimmers inhabiting coral reefs and feeding on benthic prey (Compagno, 1984). The hemiscyliids used in this study were the white spotted bamboo shark (*Chiloscyllium plagiosum*), the brown banded bamboo shark (*Chiloscyllium punctatum*), and the epaulette carpet shark (*Hemiscyllium ocellatum*). Our choice of species was based on availability in public aquaria.

The leopard sharks (*T. semifasciata*, $N = 9$) and the horn sharks (*H. francisci*, $N = 4$) were filmed at the Santa Monica Pier Aquarium in Santa Monica, CA. The three species of Hemiscyllidae (*H. ocellatum*, $N = 5$; *C. plagiosum*, $N = 24$; *C. punctatum*: $N = 21$) were filmed at the Aquarium of the Pacific in Long Beach, CA. Please note that we account for the unequal sample sizes among species in our statistical analyses by including species as a main factor. All of the live sharks used in this study were housed and maintained by aquarium staff, and thus, this project did not require the approval of the Institutional Animal Care and Use Committee at the University of California, Irvine.

TABLE 1. Summary of kinematics and morphology data collected in this study

			Kinematics		Morphology	
Order	Family	Species	N	TL (cm)	N	TL (cm)
Heterodontiformes	Heterodontidae	*Heterodontus francisci*	4	33.9–62.0	7	17.7–33.7
Carcharhiniformes	Triakidae	*Triakis semifasciata*	9	25.3–48.5	9	14.9–44.5
Orectolobiformes	Hemiscyllidae	*Chiloscyllium punctatum*	21	38.3–68.9	3	52.5–72.4
		Chiloscyllium plagiosum	24	13.0–79.8	3	80.5–85.2
		Hemiscyllium ocellatum	5	78.5–88.6	3	78.7–85.1

Ranges are given for the TL (total length, cm) for animals used in the kinematics and morphology portions of this study.

Body Curvature

To capture turning maneuvers for kinematic analysis, we used a high-definition video camera (Sony model HDR HC-5 Handycam) with a 30-Hz framing rate which was positioned approximately two meters above the water in the filming tank. Tank size differed depending on shark size. We constrained tank size and water depth to encourage sharks to make tight, planar turns, thus avoiding electroshock and other coercive methods used in previous studies. Any turns that involved touching the walls were not used for analysis. For example, *H. ocellatum*, which were up to 85 cm in total length (TL), swam in a 100 cm × 65 cm tank. At a minimum, water was 33-cm deep, which allowed animals to swim without interference from the bottom of the tank.

To increase the probability of analyzing turns of maximal body curvature, turns were defined *a priori* as a change in heading of more than 90° (Kajiura et al., 2003). Turns where the animal rolled were not used in these data sets. Video frames were analyzed at a spatial resolution of 640 × 480 pixels. This resolution was high enough to distinguish important landmarks on the shark such as eye, dorsal fin, and pectoral fins to calculate curvature. Two frames were obtained from each analyzed sequence. The first frame captured the shark's body just before the turn and the second frame captured the shark with its body at maximum curvature. Maximum curvature was defined as the posture at which the anterior tip of the rostrum was closest to the posterior tip of the caudal fin.

Body curvature has been previously quantified as a bending coefficient, BC_1:

$$BC_1 = 1 - \frac{L_1}{TL},$$

where L_1 is the minimum linear distance from the anterior tip of the rostrum to the posterior tip of the caudal fin during maximal lateral bending, and TL is the animal's TL (see Fig. 2) (Azizi and Landberg, 2002; Kajiura et al., 2003). A BC_1 of one occurs when the tip of the caudal fin is touching the tip of rostrum. Because of our concern that BC_1 might be overly influenced by the flexible caudal fin in some species, we created a second index, BC_2, that measures the curvature of the body alone:

$$BC_2 = 1 - \frac{L_2}{TL},$$

where L_2 is the minimum linear distance from the anterior tip of the rostrum to the caudal peduncle during maximal lateral bending (see Fig. 2). L_1, L_2, and TL were measured from the video frames using ImageJ software (version 1.38x, available from the National Institutes of Health). Finally, we used a third measure of body curvature, the bending angle (MBA). The angle (MBA) is formed by two lines: (1) a line from the anterior tip of the rostrum to the insertion of the first dorsal fin and (2) a line from the first dorsal fin to the caudal peduncle (Kajiura and Holland, 2002).

As mentioned above, we allowed the animals to swim and turn without provocation. The tank's physical constraints were used to elicit routine or "nonescape" turning, instead of a direct electrical or mechanical stimulus. The problem with this approach is that the body curvatures thus produced are unlikely to be at or near maximal. To increase the chances of sampling the maximum body curvature that an individual is capable of producing during routine turns, we implemented two procedures: (1) we recorded up to 30 turns for each individual, and (2) we used only the single turn with the highest curvature for each individual. Although this method is still likely to underestimate the maximal curvatures that would be seen during fast-start escape maneuvers, we reasoned that routine turning would thus provide a conservative test of our hypothesis. In other words, if we find that body shape and vertebral morphology predict the maximal body curvatures seen during routine turning, which does not require maximal muscle activation, then we provide strong indirect evidence for a mechanical relation between skeletal morphology and body motion that is also likely to hold during fast-start escape responses.

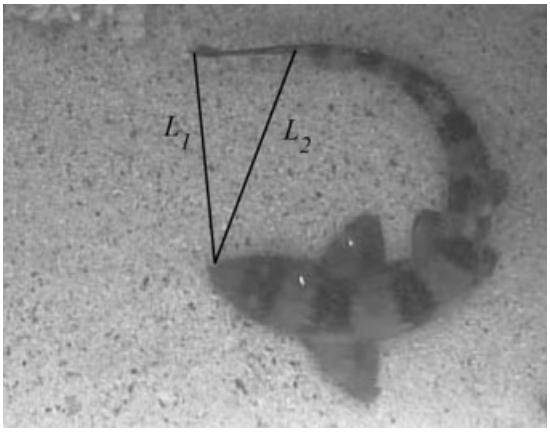

Fig. 2. Two different bending coefficients (BC) in sharks during turning. BC reported in the literature, which we denote as BC_1, is a ratio, at the time of maximal curvature, of the distance from the tip of the rostrum to the tip of the caudal fin (L_1) and the TL of the animal (Brainerd and Patek, 1998; Azizi and Landberg, 2002; Kajiura et al., 2003). To examine bending of the body independent from bending of the caudal fin, we measured BC_2—the ratio of the distance between the tip of the rostrum and the caudal peduncle (L_1) and TL.

Morphometrics

From videos (see previous section) and radiographs (below), we measured the lateral distance between the bases of pectoral fins [interpectoral fin distance (IPFD)] as a measure of body width. To calculate the fineness ratio of the body, FR_b, we took the ratio of TL and IPFD.

We measured the morphology of vertebrae, intervertebral joints, and the whole body from radiographs of museum and live specimens (Table 1, Appendix B). Radiographs were obtained from three sources. Contact radiographs of some specimens were obtained from the California Academy of Sciences, Ichthyology collection. Contact radiographs of other specimens (from the Scripps Institute of Oceanography Ichthyology collection) were taken by the authors using a cabinet radiograph (Hewlett Packard model Faxitron) and Kodak Bio-Max film. Voltage and exposure times for radiographs differed depending on the thickness of the specimen. Finally, contact radiographs of live hemiscylliids were obtained from the veterinary staff of the Aquarium of the Pacific.

From the radiographs, we examined 15 consecutive vertebrae from the pectoral girdle posteriorly (see Fig. 3). We chose this precaudal region and ignored the caudal region because the vertebrae in this region are monospondylous, and thus, are more comparable with the monospondylous vertebrae of nonelasmobranchs (Goodrich, 1930). For each of the 15 vertebrae, we used the line tool in ImageJ to measure centrum length (axial dimension, in mm) and centrum transverse width (in mm) at the face of the joint, and centrum transverse height (mm). The centrum transverse width was the same as the intervertebral joint transverse width. To measure the axial length of the 14 intervertebral joints, we measured the length of spaces between vertebrae (mm). We also measured the total number of vertebrae in each specimen.

From measurements of vertebral and intervertebral linear morphology, we calculated several other features. For centra and intervertebral joints, we calculated fineness ratios, FR_c and FR_{ij}, respectively, as the ratio of the axial length to the transverse width of the structure. Because the transverse width and

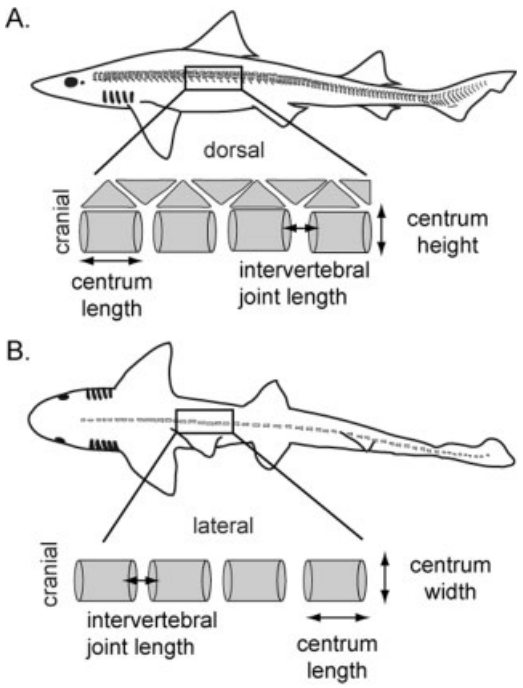

Fig. 3. Morphology of the vertebral column. For each specimen, segments of 15 vertebrae were examined from the region between the pectoral and pelvic girdles. Measurements from the centra and intervertebral joint were taken from both lateral (**A**) and dorsal (**B**) views via radiographs of each specimen. These line drawings were modified from figures in Dean and Summers (2006) and Porter et al. (2007).

height of centra were identical (see Results), we modeled the centra as circular in cross section. This allowed us to calculate the second moment of area of the centra, I_c (in mm^4), as follows:

$$I_c = \frac{\pi r^4}{4}$$

where r is the radius of the centrum, taken as the average of the height and transverse width measurements. We also measured the second moment of area of the body, I_b (in mm^4). Because shark bodies are not circular in the transverse plane, we used the following formula:

$$I_b = \frac{\pi a b^3}{4}$$

where a is the minor axis (body height) and b is the major axis (IPFD) of an ellipse, with the neutral plane of bending assumed to be the vertical septum. When calculating second moment of area as we have here, it is important to note that engineering theory assumes that the structure is homogeneous and constant in cross section. Both of these assumptions are violated with centra, as these structures taper and contain several different materials. Thus these values of I_c should be used with caution for the purposes of mechanical modeling.

Statistical Analyses

All data were tested for normal distribution using a Shapiro–Wilk W test in JMP (version 5.0.1a, SAS Institute). Only the following variables were normally distributed: BC_1, BC_2, MBA, FR_b, I_b, and TL. All the other variables were log-transformed prior to analysis: IPFD, centra length, centra width, centra height, FR_c, IVJ length, FR_j, I_b, and I_c. After transformation, all of these variables were normally distributed as judged by the Sharpiro–Wilk W. Please note that figures show untransformed data, with the exception of the figures with I_b and I_c.

To determine whether the body curvatures BC_1 and BC_2, and the body fineness ratio, FR_b, differed among species, we ran one-way ANOVAs with Student's *t*-tests for *post hoc* comparisons (JMP, version 5.0.1a, SAS Institute). For MBA and IFPD, we used TL as a covariate in separate one-way ANCOVAs (JMP, version 5.0.1a, SAS Institute). In all three cases, we ran least-squares mean Tukey's HSD for *post hoc* comparisons (Zar, 1999). Note that as we used only one turn per animal, we did not need, for that reason, to use a repeated-measures design. However, to account for the five statistical tests (one test for each of the five response variables) on the same data set, we used the Bonferroni correction with $\alpha = 0.05$ (Zar, 1999). To examine correlations among these five variables, we pooled data across species and ran eight bivariate linear regressions (JMP, version 5.0.1a, SAS Institute; see Fig. 4 for pairings). To examine size effects within the three species for which we had at least nine independent measures (*C. plagiosum*, *C. punctatum*, and *T. semifasciata*), we ran linear regressions. All *P* values for linear regressions were Bonferroni-corrected for multiple comparisons. Data are shown as a box and whisker plots where the line shows the mean for each species, the box is the 95% confidence interval, and the whiskers are the range. Letters above the plots show the significant differences among species based on *post hoc* comparisons.

Body and vertebral morphology from radiographs: To determine whether any of the morphologies differed among species, we ran one-way ANCOVAs with TL as a covariate (JMP, version 5.0.1a, SAS Institute). We ran least-squares mean Tukey's HSD comparisons, multiple comparisons for model effects (Zar, 1999). To account for multiple statistical tests (146 from 12 measurements on 15 centra per individual) on the same data set, we used the Bonferroni correction with $\alpha = 0.05$ (Zar, 1999). Data are shown as a box and whisker plots where the line shows the mean for each species, the box is the 95% confidence interval, and the whiskers are the range. Letters above the plots show the significant differences among species based on *post hoc* comparisons.

Predicting body curvature from morphology: Because our curvature and morphological data came from different animals, we paired the data sets by size-matching conspecifics using TL. To keep the mean TLs of each group statistically indistinguishable (57.8 cm vs. 55.3 cm, kinematics vs. morphology, respectively), as determined by a paired *t*-test, we selected a subset of the total data available. Out of the 63 candidate sharks, this process yielded 19 sharks for analysis, with five *T. semifasciata*, three *T. punctatum*, three *C. plagiosum*, three *H. oscillatum*, and five *H. fransci*. To determine which set of body and centra morphologies predicted body curvature, we performed mixed-direction stepwise linear regressions, with in and out *P*-values of 0.25, in JMP (version 5.01a, SAS Institute). Using all 16 of the available morphological variables from the body and all of the centra as candidate predictors, we ran three stepwise regressions with each of the curvature measures, in turn, as the dependent variable. Once the predictor set was chosen, we ran a multiple linear regression to yield the final model. To account for 15 centra used for each individual, we performed the Bonferroni correction with $\alpha = 0.05$.

RESULTS

Body Curvature During Turns

In linear regression, bending coefficient BC_2 increased with respect to increases in BC_1 (slope = 0.52; $R^2 = 0.817$; $F_{1,61} = 269.7$; $P < 0.001$) (Fig. 4A). MBA decreased significantly with respect to increases in both BC_1 (slope = −100.4; $R^2 = 0.676$; $F_{1,61} = 130.35$; $P < 0.001$) and BC_2 (slope =

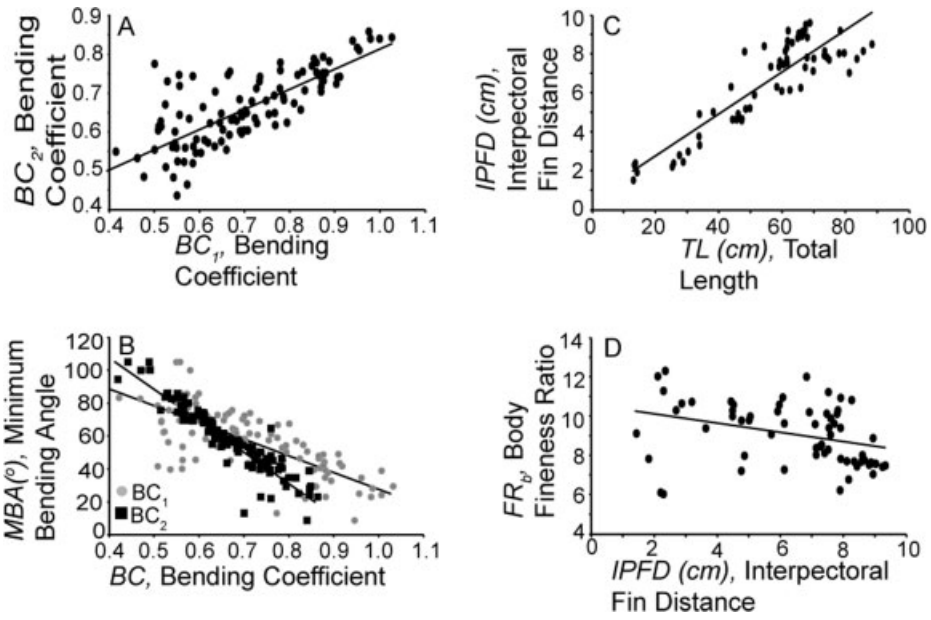

Fig. 4. Relationship of kinematic variables and body-shape morphology in sharks during turning, as determined by simple linear regression. (**A**) Bending coefficient 1 (BC_1) and bending coefficient 2 (BC_2) are significantly related ($R^2 = 0.817$; $P < 0.001$) (**B**) MBA decreases significantly with respect to both BC_1 ($R^2 = 0.676$; $P < 0.001$) and BC_2 ($R^2 = 0.767$; $P < 0.001$). (**C**) IPFD increases as TL increases ($R^2 = 0.82$; $P < 0.001$). (**D**) As shape changes from short thick bodies with low FR_b to bodies with larger FR_b values, IPFD decreases significantly ($R^2 = 0.117$; $P < 0.006$). Gray circles show measurements for BC_1 and black squares show BC_2.

-189.5; $R^2 = 0.767$; $F_{1,61} = 201.23$; $P < 0.001$) (Fig. 4B). IPFD increased significantly with respect to increasing TL, (slope = 0.105; $R^2 = 0.816$; $F_{1,61} = 210.53$; $P < 0.001$) (Fig. 4C). IPFD was weakly but significantly correlated with FR_b (slope = -0.499; $R^2 = 0.117$; $F_{1,61} = 8.073$; $P = 0.006$) (Fig. 4D).

When we represented each species by a single mean value ($N = 5$), linear regression showed BC_1 increased significantly with increases in total number of vertebrae (slope = 0.0029; $R^2 = 0.78$; $P = 0.046$). However, BC_2 regressed against total vertebral number was not significant (slope = 0.0017; $R^2 = 0.75$; $P = 0.056$). MBA was not significantly correlated with total vertebral number. Neither BC_1, BC_2, nor MBA was significantly correlated with total precaudal vertebral number.

Across species, BC_1 and MBA, but not BC_2, were significantly different as determined by ANOVA and ANCOVA after Bonferroni correction (Table 2; Fig. 5). Student's *t*-test *post hoc* contrasts show that *H. ocellatum* had the highest mean BC_1, whereas *H. francisci*, *T. semifaciata,* and *C. plagiosum* had the lowest values (Fig. 5A). As shown by *post hoc t*-tests within species, BC_1 means were greater than BC_2 means for both *C. punctatum* and *H. ocellatum*. *H. francisci* had the largest MBA, and the mean values of all other species were statistically indistinguishable (Fig. 5C). Also, taken from the video trials, three body morphologies, fineness ratio of the body, FR_b, IPFD, and TL differed significantly among species (Fig. 5D–F). *H. francisci* had the lowest of all mean FR_b values (Fig. 5D). *T. semifasciata* had a lower IPFD than all other species except *H. francisci*, with which it was statistically indistinguishable (Fig. 5E). Sharks used in this study fell into three distinct groups when we examined TL (Fig. 5F). *H. ocellatum* were significantly larger than other animals used in this study.

Regressions showed that IPFD and FR_b differed with TL, but other body curvature metrics did not differ with TL. IPFD differed significantly within species as a function of TL [(*C. plagiosum* slope = 0.0945; $R^2 = 0.96$; $F_{1,23} = 588$; $P < 0.001$), (*C. punctatum* slope = 0.1443; $R^2 = 0.90$; $F_{1,19} = 171.4$; $P < 0.001$), (*T. semifasciata* slope = 0.1127; $R^2 = 0.98$; $F_{1,7} = 327$; $P < 0.001$), respectively] (Fig. 6A). The only species showing a significant

TABLE 2. Kinematic and body shape differences among species as determined by ANOVA or ANCOVA

	DF	F	P
BC_1, Bending Coefficient	4, 58	4.85	0.012*
BC_2, Bending Coefficient	4, 58	2.75	0.216
MBA, Minimum Bending Angle	5, 57	4.09	0.018*
FR_b, Body Fineness Ratio	4, 58	28.00	<0.001*
IPFD, Interpectoral Fin Distance	5, 57	263.76	<0.001*
TL, Total Length	4, 58	9.07	<0.001*

*The *P* values are corrected for multiple tests (six) using the Bonferroni procedure at $\alpha = 0.05$. MBA and IPFD were analyzed using ANCOVA with TL as the covariate. Note the DF for ANOVA are 4, 58 whereas they are 5, 57 for ANCOVA. *Post hoc* comparisons among species are shown in figure 5.

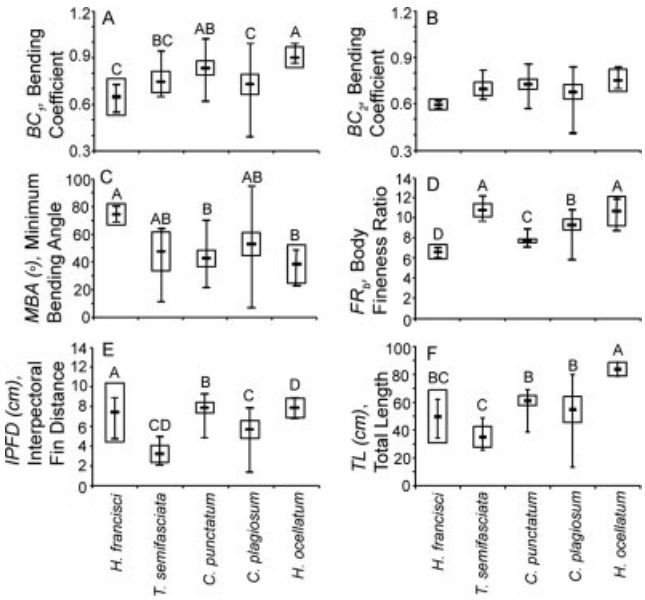

Fig. 5. Body curvature and morphology differed by species. (**A**) Bending coefficient 1 (BC_1) differed among species ($F_{4,58}$ = 4.85; P = 0.012). (**B**) Bending coefficient 2 (BC_2) did not differ significantly among species. (**C**) MBA differed significantly among species ($F_{5,57}$ = 4.09; $P < 0.018$), although *post hoc* comparisons showed the major differences were between *H. francisci* and the other species. (**D**) Fineness ratio (FR_b) of the body differed among species ($F_{4,58}$ = 28.0; $P < 0.001$). *T. semifasciata* and *H. ocellatum* have the highest FR_b of the species in this study. (**E**) IPFD differed among species ($F_{5,57}$ = 263.76; $P <$ 0.001). *Post hoc* comparisons showed that *C. punctatum* had the smaller body widths using TL as a covariate. (**F**) TL differed among species used in this study ($F_{4,58}$ = 9.07; $P < 0.0001$). On average, *H. ocellatum* are nearly twice as long as the *T. semifaciata*. Means (center mark), 95% confidence intervals (boxes), and range (vertical bars extending from means) are shown for each species. The statistics for these data can be found in Table 2. Letters above the box and whisker plots denote significant differences among species as determined by *post hoc* tests. All significance levels at 0.05 after Bonferroni correction.

relation between FR_b and TL was *C. plagiosum* (slope = 0.0385; R^2 = 0.47; $F_{1,23}$ = 19.23; $P <$ 0.001) (Fig. 6B).

Body and Vertebral Morphology

Log-transformed vertebral column morphology differed significantly among species using individual TL as a covariate after Bonferonni corrections (Table 3). Centra length differed by species when measured from both the lateral and dorsal radiographic views (Fig. 7A,B). *C. plagiosum* centra were the longest followed by *C. punctatum* then *H. ocellatum*. Centra height and width differed by species (Fig. 7C,D). *C. punctatum* centra were the highest and the widest followed by *C. plagiosum* and *H. ocellatum*, respectively. Intervertebral joint length differed by species when measured from both the lateral and dorsal radiographic views (Fig. 7E,F). Hemiscylliid joints were significantly longer than the other two species used in this study. Fineness ratios, FR_c, of vertebral centra differed by species when measured from both the lateral and dorsal radiographic views (Fig. 7G,H). The shape of the *T. semifasciata* is longer and thinner than the other species. However, intervertebral joint, FR_j, did not differ by species in the lateral and dorsal radiographic views (Fig. 7I,J). In general, the hemiscylliids (*C. punctatum, C. plagiosusm, H. ocellatum*) tended to have longer, higher, and wider structures than the other two species.

Second moment of area of vertebral centra, I_c, and also the body, I_b, differed among species using TL as a covariate after Bonferroni corrections (Table 3; Fig. 8). *C. punctatum* had the largest I_c which was nearly double the value for *H. francisci* (Fig. 8A). *H. fransici* has a larger I_b compared to *T. semifasciata* using TL as a covariate (Fig. 8B).

As shown by linear regression, I_b increased with increasing TL and changed with precaudal vertebral number after Bonferroni corrections. Two species (*H. francisci* and *T. semifasciata*) were examined over a range of sizes, and I_b increased significantly in both species as TL increased (Fig. 9A). *H. francisci* (slope = 0.0083; R^2 = 0.82; $F_{1,5}$ = 22.6, $P < 0.001$) had larger I_b than *T. semifasciata* (slope = 0.0040; R^2 = 0.95; $F_{1,7}$ = 121.48; $P <$

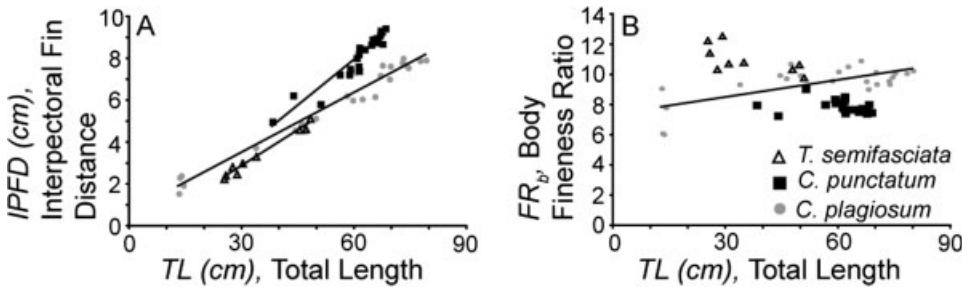

Fig. 6. Body shape changed with TL in three species, as determined by linear regression. These species were chosen for this analysis because they had adequate sample sizes for regression. (**A**) In all three species, sharks become wider (IPFD) as they grow longer (TL). (**B**) Increasing TL in *C. plagiosum* results in an overall change in fineness ratio of the body (FR_b) (R^2 = 0.47; $P < 0.001$).

TABLE 3. Vertebral column morphology and body shape differences among species as determined by ANCOVA

Variable	Aspect	DF	*F*	*P*
Centra Length	Lateral	5, 279	156.08	<0.001*
	Dorsal	5, 279	124.66	<0.001*
Centra Height		5, 279	744.70	<0.001*
Centra Width		5, 279	575.29	<0.001*
FR_c, Centra Fineness Ratio	Lateral	5, 279	32.33	<0.001*
	Dorsal	5, 279	72.87	<0.001*
I_c, Centra Second Moment of Area		5, 279	251.69	<0.001*
IVJ Length	LateraL	5, 279	35.56	<0.001*
	Dorsal	5, 279	52.28	<0.001*
FR_i, IVJ Finesness Ratio	Lateral	5, 279	3.96	0.5548
	Dorsal	5, 279	5.31	0.0584
I_b, Body Second Moment of Area		5, 19	36.11	<0.001*

*The *P* values are corrected for multiple tests (146) using the Bonferroni procedure with $\alpha=0.05$. DF for I_b are 5, 19 reflecting single measures of body shape (see Methods). *Post hoc* comparisons among species can be seen in figures 7 and 8.

0.001) for all TLs except the smallest measured. In addition, I_b did not change significantly with precaudal vertebral number (gray squares, Fig. 9B) (slope = 0.0467; R^2 = 0.796; P = 0.16) or with total vertebral number (R^2 = 0.668; P = 0.36; black squares, Fig. 9B). Neither I_b nor I_c changed significantly with changes in either BC_1 or BC_2.

Correlations

All three curvature variables—BC_1, BC_2, and MBA—were predicted by body and vertebral column morphology (Table 4). Common predictor variables, across all three models, were IPFD, TL, FR_b, centra length (lateral view), and centra height, IVJ length (lateral view only), FR_c (lateral and dorsal views), FR_j (lateral), and I_c. Four of the remaining six morphological variables were part of different models, with the exceptions of the fineness ratio of the intervertebral joint, FR_j (dorsal view), and centra length (dorsal view).

DISCUSSION

The maximal body curvature of sharks during routine turns is predicted by a combination of body and vertebral morphology, rather than by either suite of variables alone. As determined by scaled estimates in multiple regression (Table 4), vertebral morphologies are the four most important predictors of all three measures of body curvature: bending coefficient one, BC_1, bending coefficient two, BC_2, and MBA. Although we measured three times as many vertebral morphologies as compared to the number of body morphologies (12–4), random distribution of the variables would put at least three body variables in the top four for the three models (3 out of 12 across all three models). This did not occur. Instead, in all three models the first body variable enters as the fifth-most important predictor. Thus, vertebral morphology plays a dominant role in determining body curvature in these species of sharks.

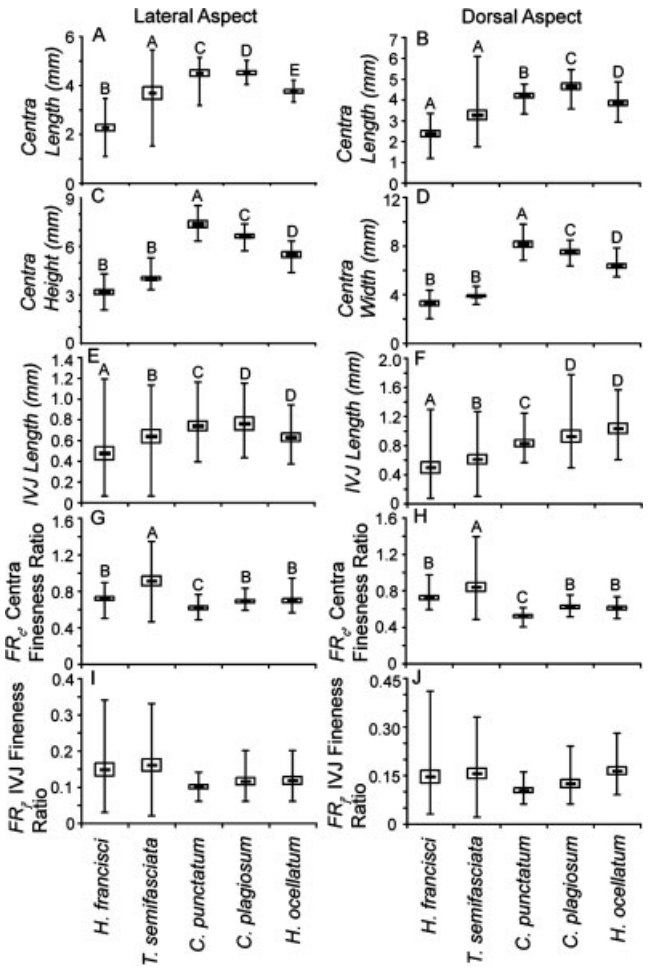

Fig. 7. Morphology of the vertebral centra and intervertebral joints as measured from both lateral and dorsal aspects in radiographs. (**A,B**) Centra length differs among species in both the lateral and dorsal aspects ($F_{5,279}$ = 156.08; $P < 0.001$ and $F_{5,279}$ = 124.66; $P < 0.001$), but there are more interspecific differences from the dorsal aspect. (**C,D**) Centra height and width differ among species and the same interspecific patterns are found in the lateral and dorsal aspects ($F_{5,279}$ = 744.70; $P < 0.001$ and $F_{5,279}$ = 575.29; $P < 0.001$). (**E,F**) Intervertebral joint length [IVJ length (mm)] differs among species but there are fewer interspecific differences than with the other morphological measures ($F_{5,279}$ = 35.56; $P < 0.001$ and $F_{5,279}$ = 52.28; $P < 0.001$). (**G,H**) Fineness ratio (FR_c) of centra differs among species ($F_{5,279}$ = 32.33; $P < 0.001$ and $F_{5,279}$ = 72.87; $P < 0.001$). (**I,J**) Intervertebral joint FR_j does not differ among species after Bonferroni corrections. Means (center mark), 95% confidence intervals (boxes), and range (vertical bars extending from means) are shown for each species. The statistics for these data can be found in Table 3. Letters above the box and whisker plots denote significant differences among species as determined by *post hoc* tests. All significance levels at 0.05 after Bonferroni correction.

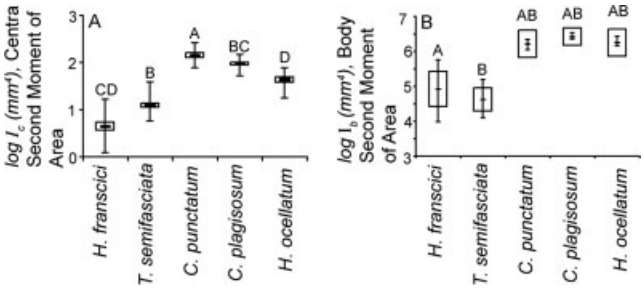

Fig. 8. Second moment of area of vertebral centra (I_c) and shark bodies (I_b). (**A**) I_c differs among species ($F_{5,279} = 251.69$; $P < 0.001$). *C. punctatum* I_c values are more than twice that of *H. fancisci* centra. (**B**) I_b differed significantly among five species of galeomorph sharks ($F_{5,19} = 36.11$; $P < 0.001$). Hemiscylliid sharks have significantly higher I_b values than the heterodontid and carcharhinid sharks. Means (center mark), 95% confidence intervals (boxes), and range (vertical bars extending from means) are shown for each species. Letters above the box and whisker plots denote significant differences among species as determined by *post hoc* comparisons. All significance levels are at 0.05 after Bonferroni correction. Data were log-transformed to normalize distributions.

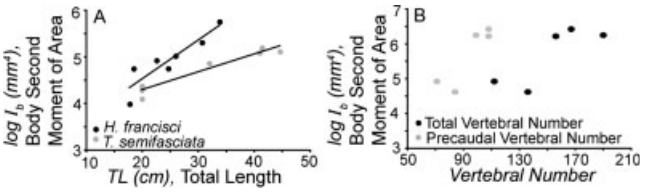

Fig. 9. Second moment of area for the centra and body (I_c and I_b) increased over a range of TLs and vertebral number. (**A**) I_b (mm^4) increased significantly over a range of TL (cm) for *H. francisci* ($R^2 = 0.82$; $P < 0.001$) and *T. semifasciata* ($R^2 = 0.95$; $P < 0.001$). In *H. francisci*, doubling shark length leads to nearly 25% increase I_b, whereas over the same size range *T. semifasciata* increased I_b by 15%. (**B**) I_b increased as total vertebral number increased, though not significantly ($R^2 = 0.668$; $P = 0.36$). However, I_b did increase significantly as the number of precaudal vertebrae increased ($R^2 = 0.796$; $P = 0.16$).

In all three models, the second moment of area of the centrum, I_c, is the most important predictor of body curvature, and centra length, lateral view, l_{cl}, is either the second- or third-most important. According to beam theory (Stevens, 1987), we expect these two variables to play an important role in determining the spring stiffness, k (in N/m), of the bending vertebral column:

$$k = \frac{3EI_c}{l_{cl}^3},$$

where E is the apparent Young's Modulus of elasticity (in Pa) of an end-loaded cantilevered beam. To our knowledge, E has never been measured during bending in elasmobranch vertebral columns. We note that k has the following proportionality with morphology:

TABLE 4. Morphology and body shape predict body curvature during routine turns

	BC_1, Bending coefficient 1			BC_2, Bending coefficient 2			MBA, Minimum bending angle		
Variable	Coefficient	Scaled estimate	*P*	Coefficient	Scaled estimate	*P*	Coefficient	Scaled estimate	*P*
IPDF, Interpectoral Fin Distance	−0.042	−0.137	0.0001	−0.413	−0.134	<0.001	11.779	38.165	<0.001
TL, Total Length	0.005	0.158	0.002	0.003	0.086	0.002	−1.718	−51.894	<0.001
FR_b, Body Fineness Ratio	−0.069	−0.171	<0.001	−0.048	−0.12	<0.001	15.034	37.586	<0.001
I_b, Body Second Moment of Area	−0.075	−0.085	0.013	–	–	–	30.698	34.228	<0.001
Total Vertebral Number	0.002	0.116	0.0001	0.001	0.073	<0.001	–	–	–
Centra Length (lateral)	−0.263	−0.519	<0.0001	−0.169	−0.334	<0.001	41.672	82.198	<0.001
Centra Height	−0.146	−0.441	0.0009	−0.115	0.347	0.0003	35.453	107.495	<0.001
IVJ Length (lateral)	0.212	0.12	0.0587	0.211	0.119	0.002	−31.23	−17.644	0.0364
Centa Length (dorsal)	–	–	–	–	–	–	–	–	–
Centra Width	–	–	–	–	–	–	−23.326	−9.061	0.154
IVJ Length (dorsal)	–	–	–	–	–	–	−6.031	−5.06	0.079
FR_c, Centra Fineness Ratio (lateral)	1.015	0.447	<0.0001	0.646	0.284	<0.001	−161.777	−71.181	<0.001
FR_e, Centra Fineness Ratio (dorsal)	−0.117	−0.058	0.0172	−0.063	−0.031	0.0343	13.912	6.852	0.036
FR_j, IVJ Fineness Ratio (lateral)	−0.698	−0.115	0.1378	−0.779	−0.128	0.006	100.537	16.538	0.107
FR_j, IVJ Fineness Ratio (dorsal)	–	–	–	–	–	–	–	–	–
I_c, Centra Second moment of Area	0.882	0.957	<0.001	0.595	0.646	<0.001	−176.24	−191.31	<0.001
Whole model	*P* <0.0001	R^2 0.523		P <0.0001	R^2 0.537		*P* <0.0001	R^2 0.584	

Stepwise linear regression was used to determine which varibles would be included in each model. Variables not included in a model are shown as –. Variables overlayed with gray are excluded from one or more of the models. Coeffecients, scaled estimates, and *P* value are reported for each variable in each model. Note that variables may be included in the stepwise procedure that are not neccessarily significant.

$$k \propto \frac{I_c}{l_{cl}^3}.$$

With this relation in mind, we might expect that the vertebral columns with the smallest values of k, assuming here that E is constant among individuals and species, are the ones correlated with the largest body curvatures. The opposite is the case. As shown by the signs of the coefficients and scaled estimates of I_c and the lateral length of the centra, l_{cl} (Table 4), increases in k are proportional to increases in body curvature. (Recall that BC_1 and BC_2 get larger as bending increases and MBA gets smaller.)

Why does it appear that k increases with increasing body curvature? This relationship may be erroneous. Body stiffness, as measured by Young's modulus of elasticity, E, is inversely proportional to body curvature, as measured by propulsive wavelength, during steady swimming in physical models of fish (McHenry et al., 1995). Thus, E may vary inversely with increasing I_c, canceling out any increase in k. Another option is that E increases with increasing I_c, which would amplify the effect. That option, along with the alternative that E may be constant, we find most intriguing. If, as these morphological data suggest, the k of the vertebral column increases with increasing body curvature, sharks with high-curvature will store more elastic strain energy in their vertebral columns than do the low-curvature sharks. At first blush, this result is counterintuitive: sharks with stiffer vertebral columns should bend less than those with less stiff vertebral columns. However, that model assumes that the capacity of the muscles to produce bending moments remains constant as the vertebral column changes. If that is not the case, and bending moment capacity increases as the vertebral column increases stiffness, the additional elastic energy could be used for powering the propulsive phase of the turn. This would occur in much the same way that elastic energy storage in the skin appears to help power the propulsive phase of fast starts in *Polypterus palmus* (Westneat et al., 1998) and *Polypterus senegalus* (Tytell and Lauder, 2002). Mechanically, we predict that combining elastic energy from the first phase of turning with the muscular output from the second phase would double the power output of the shark at that moment. This prediction could be tested by measuring the acceleration of different individuals as they take the second half-tailbeat coming out of the turn.

Another counter-intuitive aspect of these results is that the precaudal vertebral segments we measured, with only 15 vertebrae and 14 joints running caudally from the pectoral girdle, have morphologies that are correlated with the bending curvature of the whole vertebral column and body. In our specimens, the number of vertebrae between the pectoral and pelvic girdles ranged from 19 to 26 (our counts), and the total number of vertebrae ranged from 88 to 190 (Springer and Garrick, 1964). We posit two likely explanations for the correlation. First, the measured precaudal vertebrae may be only minimally involved in a mechanism causing whole-body curvature, and their predictive power comes from intra-individual correlations among the serially homologous elements of the vertebral column. Alternatively, the measured precaudal vertebrae may play a more direct role in a mechanism that bends the whole body. On the basis of the correlation of body curvature during steady swimming and bending stiffness of the axial skeleton in white sturgeon, *Acipenser transmontanus*, the precaudal section may allow muscle to generate high force by offering passive antagonism (Long, 1995). In this same mid-body region, the greatest muscle-generated bending moments may occur, according to a dynamic beam model of a swimming saithe, *Pollachius virens* (Cheng et al., 1998). Given these lines of evidence, we favor this explanation that the precaudal vertebral column is mechanistically involved in generating whole-body curvature.

One potential problem with this study is that we are not measuring body curvatures of the magnitude seen during fast-start escape responses. In fast starts, we would likely see a much stronger correlation between morphology and body curvature than the one we report here. It is also possible at the limit of performance that the pattern of correlations might be quite different, given the different loading conditions. In this study, we have attempted to measure the highest curvatures observed during routine turns. We used a definition of turning—rotating at least 90° in the horizontal plane—that removed by truncation all low-curvature turns. Also, we screened all of the remaining turns from each individual and used only the one, maximal-curvature turn from each, thus increasing the probability of capturing the maximal or near-maximal turn that an individual is capable of producing under these circumstances. We found that our mean values for BC_1 among our species range from a low of 0.65 to a high of 0.91 (see Fig. 5). This range is over and above the only other BC_1 values available for sharks: ~0.46 for fast-starting *Squalus acanthias* (measured from Fig. 1 of Domenici et al., 2004), and 0.57, 0.59, and 0.64 for *Carcharhinus plumbeus*, *Sphyrna tiburo*, and *Sphyrna lewini*, respectively (mean values during "sharp turning" following electrical stimulation, Kaijura et al., 2003).

When we examined how body curvature differed among species (see Fig. 5), we found that only the two measures that included the whole length of the fish, BC_1 and MBA, differed significantly (Table 2). This demonstrates that the metric chosen for body curvature affects the results. Measurements of BC_1 and MBA, as whole-body indices, overestimate curvature of the body anterior to the

caudal fin. Researchers should keep this in mind when selecting whole-body indices of curvature. Moreover, we have shown that BC_2 is correlated with BC_1 and MBA (see Fig. 4), even though it measures a different feature of body curvature. We note that these correlations, among species and curvature and among different curvature measures, may be influenced by phylogenetic correlation. With more species, we would be able to measure those effects directly using independent contrasts (Felsenstein, 1985).

Body shape influences the ability of sharks to maneuver (Weihs, 1981). We found that body shape differed among species (Figs. 5 and 8; Tables 2 and 3). Body shape was discriminated best by fineness ratio, FR_b, the ratio of total body length, TL, to body width as measured by the IPFD, with four of the five species having significantly different means. Compared with FR_b, neither TL nor IPFD discriminated body shape as well, with three groups and two pairs statistically indistinguishable, respectively (see Fig. 5). Moreover, although TL and IPFD were significantly correlated within each of the three species for which we had large sample sizes, FR_b was significantly correlated with TL in only one species (see Fig. 6). We argue that although FR_b is derived from TL and IPFD, it acts as an independent shape metric rather than a simple amalgam of its constituents. This is in agreement with data on bony fish vertebral column morphology, in which FR_c was a better predictor than either metric alone (Ward and Brainerd, 2007). Showing less discriminatory power than any of these three metrics, the mean values of the second moment of area of the body, I_b, a function of IPFD, and height of the body, separated into only two statistically independent groups (see Fig. 8). In spite of its lack of differences among species, I_b was a significant predictor of BC_1 and MBA when data were pooled across species (Table 4). In addition, within two species for which we had sufficient sample sizes to run regressions, I_b increased significantly with increasing TL (see Fig. 9). This same trend was found in two different shark species, *Carcharhinus plumbeus* and *Sphyrna lewini* (Kaijura et al., 2003). The correlations between morphologies and TL are, within species, likely to have a strong ontogenetic component and the potential to scale body curvature allometrically.

With data pooled across species, our multiple regression models explain more than 50% of the variance (R^2 value) in body curvature during routine turns (Table 4). This compares favorably with the 70% explained by the number of functional intervertebral joints in four species of bony fish during C-starts (Brainerd and Patek, 1998). We found that the total vertebral number was a significant predictor of BC_1 and BC_2 in our study species (Table 4). Even if we look at the mechanical influence of just the vertebral column on whole-body bending, the number of vertebrae is but one feature that may influence the properties—such as stiffness, energy storage, and energy loss—that determine mechanical behavior. For instance, material properties of vertebral centra have been shown to differ by species (Porter et al., 2006, 2007). Bending properties of the intervertebral joints influence flexibility in blue marlin, *Makaira nigricans* (Long, 1992). In elasmobranchs, intervertebral joint stiffness may vary as determined by changes in hydrostatic pressure within the joint capsule (Home, 1809).

What explains the other 50% of the variance in curvature? Clearly, the anatomy, activity patterns, and contractile properties of muscle determine much of body curvature during swimming. Anatomically, the passive properties of the musculotendinous system provide a large degree of stiffness to the bending body in hagfish, *Myxine glutinosa* (Long et al., 2002) and control the distribution of muscular force in elasmobranchs (Donley et al., 2004; Gemballa et al., 2006; Shadwick and Gemballa, 2006). In terms of activity patterns, red muscle in *T. semifasciata* is activated along the entire length of the shark's body, contributing to power production during swimming (Donley and Shadwick, 2003). Finally, contractile properties of shark muscle provide high mechanical power output over a range of temperatures and bending frequencies (Bernal et al., 2001, 2005).

Summary

To our knowledge, this is the first study that shows a significant correlation between the morphology of the vertebral column and body curvature in sharks while swimming (Wilga and Lauder, 2004; Webb, 2006). The most important vertebral morphologies—the second moment of area and the length of the centra—are those related to the mechanics of bending, providing a hypothetical functional link between spring stiffness and body curvature. However, many mechanical aspects of cartilaginous vertebral columns, especially the elastic moduli of the intervertebral joints, have yet to be studied and are likely to have significant effects on shark flexibility.

ACKNOWLEDGMENTS

The authors thank the staff at the Santa Monica Pier Aquarium in Santa Monica, CA (Jose Bacallo), and the Aquarium of the Pacific in Long Beach, CA (Dr. Lance Adams, Perry Hampton, and Steve Blair), for allowing us to film animals in their live collections. They provided assistance to this project in numerous ways. Jeff Landesman and the Cabrillo Marine Aquarium in San Pedro, CA, allowed us to test our data collection methods. Ruth Porter, Jessica Alvarez, Nick Tan, Sabreena

Kasbati, and Andrew Clark assisted during filming. Matt Talluto provided useful insight into statistical models. This manuscript was improved by comments from Hannah Rosenblum and Thomas Kleinteich as well as by two anonymous reviewers. Line drawings from Figure 3 are the courtesy of Andrew Clark. Josh de Leeuw and the Biomechanics Group at UCI have provided constant support, input, and development of this project. Funding was provided with grants from the Society of Integrative and Comparative Biology and American Elasmobranch Society to MEP, and the National Science Foundation to Adam Summers (IBM 0317155) and JHL (DBI 0442269).

LITERATURE CITED

Azizi E, Landberg T. 2002. Effects of metamorphosis on the aquatic escape response of the two-lined salamander (*Eurycea bislineata*). J Exp Biol 205:841–849.

Bernal D, Dickson KA, Shadwick RE, Graham JB. 2001. Review: Analysis of the evolutionary convergence for high performance swimming in lamnid sharks and tunas. Comp Biochem Physiol Part A 129:695–726.

Bernal D, Donley JM, Shadwick RE, Syme DA. 2005. Mammal-like muscles power swimming in a cold-water shark. Nature 437:1349–1352.

Brainerd EL, Patek SN. 1998. Vertebral column morphology. C-start curvature, and the evolution of mechanical defenses in Tetraodontiform fishes. Copeia 4:971–984.

Cheng JY, Pedley TJ, Altringham JD. 1998. A continuous dynamic beam model for swimming fish. Philos Trans: Biol Sci 353:981–997.

Compagno LJV. 1984. Sharks of the World: An Annotated and Illustrated Catalogue of Shark Species Known to date. Rome: United Nations Development Programme.

Compagno LJV. 2003. Sharks of the Order Carcharhiniformes. Caldwell, NJ: Blackburn Press.

Daniel TL. 1984. Unsteady aspects of aquatic locomotion. Amer Zool 24:121–134.

Dean MN, Summers AP. 2006. Cartilage in the skeleton of cartilaginous fishes. Zool 109:164–168.

Domenici P, Standen EM, Levine RP. 2004. Escape manoeuvers in the spiny dogfish (*Squalus acanthias*). J Exp Biol 207:2339–2349.

Donley JM, Sepulveda CA, Konstandinidis P, Gemballa S, Shadwick RE. 2004. Convergent evolution in mechanical design of lamnid sharks and tunas. Nature 429:61–65.

Donley JM, Shadwick RE. 2003. Steady swimming muscle dynamics in the leopard shark *Triakis semifasciata*. J Exp Biol 206:1117–1126.

Felsenstein J. 1985. Phylogenies and the comparative method. Am Nat 125:1–15.

Gemballa S, Konstantinidis P, Donley JM, Sepulveda C, Shadwick RE. 2006. Evolution of high-performance swimming in sharks: Transformations of the musculotendinous system from subcarangiform to thunniform swimmers. J Morphol 267:477–493.

Goodrich ES. 1930. Studies on the structure and development of vertebrates. London: Macmillan.

Herrel A, Grauw ED, Lemos-Espinal JA. 2001. Head shape and bite performance in Xenosaurid lizards. J Exp Zool 290:101–107.

Home E. 1809. On the nature of the interverterbal substance in fish and quadrupeds. Philos Trans R Soc 99, 177–187.

Kajiura SM, Forni JB, Summers AP. 2003. Maneuvering in juvenile carcharhinid and sphyrnid sharks: The role of the hammerhead shark cephalofoil. Zool 106:19–28.

Kajiura SM, Holland KN. 2002. Electroreception in juvenile scalloped hammerhead and sandbar sharks. J Exp Biol 205:3609–3621.

Lindsey CC. 1978. Form, function, and locomotory habits in fish. In: Boar WS, Randalll DJ, editors. Fish Physiology, Vol. 7. New York: Academic Press. pp 1–100.

Long JH Jr. 1992. Stiffness and damping forces in the intervertebral joints of blue marlin (*Makaira nigricans*). J Exp Biol 162:131–155.

Long JH Jr. 1995. Morphology, mechanics, and locomotion—the relation between the notochord and swimming motions in sturgeon. Environ Biol Fishes 44:199–211.

Long JH Jr, Koob-Emunds M, Sinwell B, Koob TJ. 2002. The notochord of hagfish *Myxine glutinosa*: Visco-elastic properties and mechanical functions during steady swimming. J Exp Biol 205:3819–3831.

Long JH Jr, Nipper KS. 1996. The importance of body stiffness in undulatory propulsion. Am Zool 36:678–694.

Maisey JG, Naylor GJP, Ward DJ. 2004. Mesozoic elasmobranchs, neoselachian phylogeny and the rise of modern elasmobranch diversity. In: Arratia G, Tintori Am, editors. Mesozoic Fishes 3- Systematics, Paleoenvironments, and Biodiversity, Vol. 3. Munich, Germany: Verlag. pp 17–56.

McHenry MJ, Pell CA, Long JH Jr. 1995. Mechanical control of swimming speed: Stiffness and axial wave form in undulating fish models. J Exp Biol 198:2293–2305.

Porter ME, Beltrán JL, Koob TJ, Summers AP. 2006. Material properties and biochemical composition of mineralized vertebral cartilage in seven elasmobranch species (Chondrichthyes). J Exp Biol 209:2920–2928.

Porter ME, Koob TJ, Summers AP. 2007. The contribution of mineral to the material properties of vertebral cartilage from the smooth-hound shark *Mustelus californicus*. J Exp Biol 210:3319–3327.

Root RG, Courtland HW, Shepherd W, Long JH Jr. 2007. Flapping flexible fish: Periodic and secular body reconfigurations in swimming lamprey, *Petromyzon marinus*. Exp Fluids 43:779–797.

Shadwick RE, Gemballa S. 2006. Structure, kinematics, and muscle dynamics in undulatory swimming. In: Shadwick RE, Lauder GV, editors. Fish Biomechanics, Vol. 23. San Diego: Academic Press. pp 241–274.

Springer VG, Garrick JAF. 1964. A survery of vertebral numbers in sharks. Proc US Nat Mus 116:73–96.

Stevens KK. 1987. Statics and Strength of Materials, 2nd ed. NJ: Prentice-Hall.

Summers AP, Long JH Jr. 2006. Skin and bones, sinew and gristle: The mechanical behavior of fish skeletal tissues. In: Shadwick RE, Lauder GV, editors. Fish Biomechanics, Vol. 23. Academic Press. pp 141–177

Tytell ED, Lauder GV. 2002. The C-start escape response of *Polypterus senegalus*: Bilateral muscle activity and variation during stage 1 and 2. J Exp Biol 205:2591–2603.

Wainwright SA, Biggs WD, Currey JD, Gosline JM. 1976. Mechanical Design in Organisms. Princeton: Princeton University Press.

Ward AB, Brainerd EL. 2007. Evolution of axial patterning in elongate fishes. Biol J Linn Soc 90:97–116.

Webb PW. 1975. Hydrodynamics and energetics of fish propulsion. Bull Fish Bd Can 190:1–159.

Webb PW. 2006. Stability and manveuverability. In: Shadwick RE, Lauder GV, editors. Fish Biomechanics, Vol. 23. San Diego, CA: Elsevier Academic Press.

Weihs D. 1981. Body section variations in sharks—an adaptation for efficient swimming. Copeia 1981:217–219.

Westneat MW, Hale ME, McHenry MJ, Long JH Jr. 1998. Mechanics of the fast-start: Muscle function and the role of intramuscular pressure in the escape behavior of *Amia calva* and *Polypterus palmas*. J Exp Biol 201:3041–3055.

Wilga CD, Lauder GV. 2004. Biomechanics of locomotion in sharks, rays, and chimeras. In: Carrier JC, Musick JA, Heithaus MR, editors. Biology of Sharks and Their Relatives. Boca Raton: CRC Press. pp 139–164.

Zar JH. 1999. Biostatistical Analysis. NJ: Prentice Hall.

APPENDIX A: A KEY TO ABBREVIATIONS USED IN THIS STUDY

Abbreviation	Name	Units
BC_1	Bending Coefficient, including caudal fin	–
BC_2	Bending Coefficient, excluding caudal fin	–
MBA	Minimum Bending Angle	degrees
FR_b	Body Fineness Ratio	–
IPFD	Interpectoral Fin Distance	cm
TL	Total Length	cm
FR_c	Centra Fineness Ratio	–
FR_i	IVJ Fineness Ratio	–
IVJ	Intervertebral joint	–
I_c	Centra Second Moment of Area	mm^4
I_b	Body Second Moment of Area	mm^4

APPENDIX B: SPECIMENS FROM THE MORPHOLOGY PORTION OF THIS STUDY WERE EXAMINED USING CONTACT RADIOGRAPHS OBTAINED FROM THE CALIFORNIA ACADEMY OF SCIENCES (CAS), SCRIPPS INSTITUTE OF OCEANOGRAPHY ICHTHYOLOGY COLLECTION (SLO), OR FROM LIVE ANIMALS RADIOGRAPHED AT LONG BEACH AQUARIUM OF THE PACITIC (LBAOP)

Order	Family	Species	Collection	Number	TL (mm)
Carcharhiniformes	Triakidae	*Triakis semifasciata*	CAS	SU15267	445.0
			CAS	SU15268-r	406.0
			CAS	SU15269-r	412.0
			SIO	H 51-71	358.0
			SIO	60-77-5A	333.1
			SIO	60-77-5A	213.4
			SIO	60-77-5A	240.2
			SIO	60-77-5A	222.7
			SIO	60-77-5A	196.1
Heterodonitformes	Heterodontidae	*Heterodontus francisci*	CAS	19176-rHf	336.6
			CAS	19176-rHf	308.3
			CAS	SU09059-r	249.9
			SIO	75-654	265.7
			SIO	75-654	176.9
			SIO	59-301 5A	226.0
			SIO	59-301 5A	185.0
Orectobiformes	Hemiscyllidae	*Chiloscyllium plagisosum*	LBAOP	–	852.0
			LBAOP	–	815.0
			LBAOP	–	805.0
		Chiloscyllium punctatum	LBAOP	–	680.0
			LBAOP	–	724.0
			LBAOP	–	525.0
		Hemiscyllium ocellatun	LBAOP	–	836.0
			LBAOP	–	787.0
			LBAOP	–	851.0